ACS OMEGA

Open Access

http://pubs.acs.org/journal/acsodf

Article

Simultaneous Removal of As(iii) and As(v) from Aqueous Solution by Using Iron-Functionalized Polythiophene: A Novel Approach toward Water Treatment

Rupkamal Chetia, Shrutipriya Devi, Nishant Shukla, Abhishek Hazarika, Shreemoyee Bordoloi, Binod Pokhrel, Binoy K Saikia, Ankur Gogoi,* and Surajit Konwer*

Cite This: *ACS Omega* 2024, 9, 37012−37024

Read Online

ACCESS | Metrics & More | Article Recommendations | Supporting Information

ABSTRACT: Arsenic contamination in groundwater poses a significant threat to human health, affecting millions worldwide. This study presents a novel approach for simultaneous remediation of both As(III) and As(V) by using iron-functionalized polythiophene (PTh@Fe) composites. The PTh@Fe composite was synthesized by a reduction process involving $FeCl_2/FeCl_3$ byproducts of polymerization, resulting in a highly efficient adsorbent for both As(III) and As(V) species. The investigation systematically examined key parameters influencing arsenic removal, including adsorbent dosage, pH, initial arsenic concentration, and contact time. The composite exhibited exceptional adsorption capacities, with maximum removal percentages of 98.7% for As(III) and 98.8% for As(V) under the optimized conditions. Thermodynamic and kinetic analyses suggested endothermic and spontaneous adsorption processes following a pseudo 2nd-order mechanism. Furthermore, the Langmuir isotherm model provided an excellent fit to the experimental data, with maximum adsorption capacities of 8.62 mg/g for As(V) and 7.57 mg/g for As(III). Density functional theory (DFT) calculations confirmed the feasibility of arsenic adsorption onto iron species in various oxidation states, offering valuable theoretical insights into the process. Furthermore, the composite demonstrated good reusability over multiple adsorption−desorption cycles and tolerance to coexisting anions, highlighting its practical applicability for water purification. This research demonstrates the potential of iron-functionalized polythiophene composites as a promising solution for addressing arsenic contamination in water sources, bridging the gap between innovative materials and theoretical understanding in environmental science and water treatment technologies.

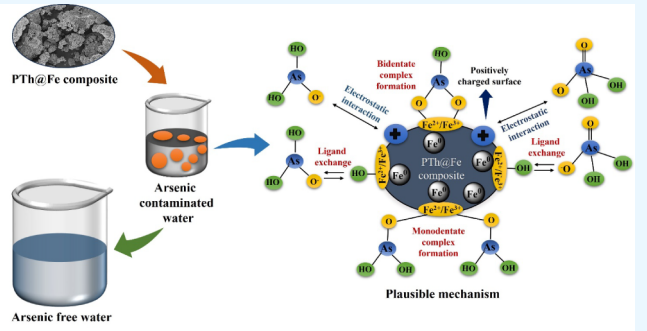

1. INTRODUCTION

Contamination of arsenic in water bodies poses a severe threat to individuals who rely on groundwater to meet their water needs. High levels of arsenic in groundwater have been documented in numerous countries, including Indian states.[1−4] Alarmingly, around 200 million people are exposed to arsenic-contaminated water annually, exceeding the World Health Organization's recommended limit of 10 $\mu g\ L^{-1}$.[5−7] Consuming arsenic-laden water can cause cancers and noncancerous health issues like skin changes, cardiovascular diseases, and hypertension.[8−10]

Arsenic contamination comes from natural sources and human activities. In water, it mainly exists as arsenite (+3) and arsenate (+5). Arsenite [As(III)] is more mobile and toxic than arsenate [As(V)], which is found in surface water under aerobic conditions, while arsenite is common in groundwater under anaerobic conditions. Organic arsenic is generally less hazardous than inorganic arsenic. At neutral pH, As(V) exists as $H_2AsO_4^-$ and $HAsO_4^{2-}$, while As(III) exists as H_3AsO_3.[11−13]

Various strategies to remove arsenic from water include coagulation, oxidation, reverse osmosis, adsorption, membrane filtration, and ion exchange.[5,14,15] However, methods like reverse osmosis and ion exchange are impractical due to low efficiency, toxic waste, and high costs. In contrast, adsorption, alongside precipitation methods, finds frequent use in arsenic removal, especially in developing nations. Precipitation produces large amounts of sludge, making adsorption the preferred method due to its simplicity, cost-effectiveness, minimal toxic waste, and efficiency at low contaminant levels.[16]

Iron oxide-based adsorbents are popular in research due to their availability, sustainability, and cost-effectiveness. Recent

Received: April 3, 2024
Revised: August 2, 2024
Accepted: August 9, 2024
Published: August 22, 2024

https://doi.org/10.1021/acsomega.4c03184
ACS Omega 2024, 9, 37012−37024

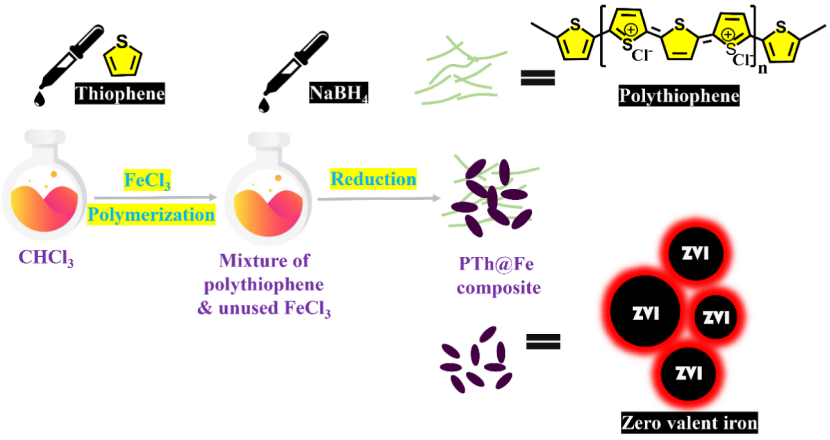

Figure 1. Schematic representation for the synthesis of PTh@Fe composite.

efforts aim to provide clean water to remote, rural, and disadvantaged communities.[17] In this endeavor, metallic iron (ZVI) is a promising, affordable material for water treatment due to its reactive surface and large area. However, ZVI has limitations like instability, rapid aggregation, and difficulty in separating from treated water.[18−24]

To overcome these challenges, immobilizing ZVI on materials like activated carbon, clay, biochar, resin, and zeolite has been proposed.[25,26] This enhances ZVI's stability and preserves its qualities. However, the majority of them were capable of just moderately successful in eliminating arsenic. Therefore, there is a need for further research to identify novel, efficient support matrices for ZVI that can achieve high arsenic removal efficiency.

Recently, conducting polymers like polypyrrole (PPy),[27,28] polyaniline (PANI),[29,30] and polythiophene (PTh)[31,32] have gained attention for their effective heavy metal adsorption and recyclability. Polythiophene, in particular, stands out due to its unique properties and environmental benefits. PTh interacts with heavy metals due to its sulfur atoms with lone pairs.[33] It undergoes protonation and deprotonation in acidic or alkaline solutions, changing its surface charge and involving ion doping.[34] Our previous research demonstrated PTh's effectiveness in arsenic removal.[35] Therefore, using PTh as a support for iron oxide and zerovalent iron (ZVI) particles for arsenic removal from polluted water is promising.

In this research, we developed a novel composite material, iron-functionalized polythiophene (PTh@Fe), using $FeCl_2$/$FeCl_3$ as the iron source and sodium borohydride for reduction. The study focused on the composite's properties and its effectiveness in removing As(V) and As(III) from water. We thoroughly examined the adsorption behavior of PTh@Fe grains under various conditions. Advanced techniques like X-ray photoelectron spectroscopy (XPS) and density functional theory (DFT) were used to understand the arsenic removal mechanisms. This study is pioneering in demonstrating the arsenic adsorption capabilities of PTh@Fe composites, offering significant potential for environmental science and water purification. It is worth noting that, to the best of our knowledge, no prior research findings exist regarding the arsenic adsorption capabilities of these highly efficient iron-functionalized polythiophene composites.

2. EXPERIMENTAL METHODS

2.1. Materials. In this study we exclusively utilized analytical-grade chemicals, and all solutions were prepared using double-distilled water. Thiophene was sourced from Spectrochem PVT. Ltd., Mumbai, India. Chloroform ($CHCl_3$) and sodium borohydride ($NaBH_4$) were obtained from Finar Chemicals, Gujarat, India. Anhydrous ferric chloride ($FeCl_3$) was procured from Qualikems Fine Chem Pvt. Ltd., Vadodara, India. Ethanol was obtained from Analytical CSS Reagent, Jiangshu Province. Sodium arsenite ($NaAsO_2$) and sodium arsenate ($Na_2HAsO_4{\cdot}7H_2O$) were procured from Loba Chemie Pvt Ltd., Wodehouse Road, Mumbai, India.

Stock solutions of As(III) and As(V) were prepared at a concentration of 100 mg/L. For the As(III) solution, 0.087 g of $NaAsO_2$ salt was dissolved in a 500 mL volumetric flask filled with double-distilled water. Similarly, for the As(V) solution, 0.208 g of $Na_2HAsO_4{\cdot}7H_2O$ salt was dissolved in a 500 mL volumetric flask with double-distilled water. These stock solutions were then diluted as needed for various experiments. The concentrations of the stock solutions and the residual arsenic after adsorption experiments were measured using an atomic absorption spectroscopy (AAS) instrument. The AAS was calibrated with standard solutions for accuracy, and the arsenic concentrations in mg/L were recorded.

2.2. Preparation. PTh@Fe composite was synthesized by through an in situ polymerization technique utilizing $FeCl_3$ as the oxidizing agent (Figure 1). Initially, in a 250 mL conical flask, 5 g of ferric chloride was introduced, followed by the addition of 80 mL of chloroform. The mixture was stirred for 10 min using a magnetic stirrer at 500 rpm. Subsequently, 5 mL of thiophene was added dropwise while maintaining constant stirring for the next 4 h to ensure complete polymerization. The polymerization byproduct, consisting of $FeCl_2$ and/or $FeCl_3$, served as the source of iron for ZVI synthesis. A freshly prepared 1 M $NaBH_4$ solution (100 mL) was slowly added to the mixture within an N_2 atmosphere, resulting in the formation of ZVI. The resulting mixture was stirred for 30 min to ensure the complete reduction of the iron sources. The resulting product (PTh@Fe) was thoroughly washed multiple times with ethanol and DI water, followed by drying in a vacuum oven at 60 °C for the subsequent 24 h.

2.3. Analytical Characterization. The surface morphology of PTh, PTh@Fe (untreated/treated) was examined using a scanning electron microscope (SEM) made by Carl ZEISS Microscopy, Germany, model ZEISS, SIGMA. Fourier-trans-

https://doi.org/10.1021/acsomega.4c03184
ACS Omega 2024, 9, 37012−37024

form infrared (FTIR) spectra of the samples were acquired using the PerkinElmer Spectrum-Two instrument. The X-ray diffraction (XRD) patterns of the samples were recorded using the ULTIMA IV instrument (Rigaku).

For the analysis of chemical bonding and environment, X-ray photoelectron spectra (XPS) of PTh@Fe (both As treated and untreated), the XPS spectrometer (ESCALAB Xi+; Thermo Fisher Scientific) was employed. The residual concentration of arsenic (As) was quantified using an atomic absorption spectrometer (Thermo Scientific AAS model AA 303).

2.4. Batch Experiment. Equilibrium adsorption capacity (q_e) and % removal efficiency was calculated using eqs 1 and 2 respectively.

$$q_e = \frac{C_i - C_e}{W} \times V \tag{1}$$

$$\text{Removal efficiency}(\%) = \frac{C_i - C_e}{C_i} \times 100 \tag{2}$$

where q_e represents the adsorption capacity (mg/g). The term C_i and C_e demonstrates the initial and equilibrium arsenic concentrations (mg/L), respectively. The volume (L) of the solution and mass (g) of the adsorbent are represented by V and W respectively.

The equilibrium adsorption behavior of arsenic was described using two models: the Langmuir isotherm and the Freundlich isotherm. Langmuir's adsorption isotherm model is represented by eq 3, and its linear form is given by eq 4.

$$q_e = \frac{q_{max} K_L C_e}{1 + K_L C_e} \tag{3}$$

$$\frac{1}{q_e} = \frac{1}{K_L q_{max}} \frac{1}{C_e} + \frac{1}{q_{max}} \tag{4}$$

Here, K_L (L/mg) represents the Langmuir isotherm constant, while by q_{max} (mg/g), denotes the maximum adsorption capacity. K_L reflects the binding affinity between the arsenic species and the adsorbent.

(eq 5) is used to determine the separation factor (R_L).

$$R_L = \frac{1}{1 + C_i \times K_L} \tag{5}$$

In the given equation, R_L stands for the Langmuir constant, which indicates the nature of adsorption as either irreversible ($R_L = 0$), linear ($R_L = 1$), favorable ($0 < R_L < 1$) or unfavorable ($R_L > 1$).

(eq 66) represents Freundlich's adsorption isotherm model and (eq 7) represents its linear form.

$$q_e = K_f C_e^{1/n} \tag{6}$$

$$\log q_e = \log K_f + \frac{1}{n} \log C_e \tag{7}$$

K_f represents the Freundlich constant. In this equation, ($1/n$) denotes the adsorption intensity, and its value determines the favorability of the adsorption process, with values between 0.1 and 0.5 indicating favorability, while values above 2 suggest unfavorability.

To assess the rate of arsenic adsorption on the synthesized adsorbent, we employed both pseudo 1st-order and pseudo 2nd-order kinetic models. eq 8 represents the pseudo1st-order kinetic model.

$$\ln(q_e - q_t) = \ln q_e - K_1 t \tag{8}$$

At time t, the adsorption capacity (mg/g) is denoted as q_t in the equation. The parameter K_1 (min^{-1}) signifies the equilibrium rate constant.

The rate equation for Pseudo 2nd order is expressed in eq 9.

$$\frac{t}{q_e} = \frac{1}{K_2 q_e^2} + \frac{1}{q_e} \tag{9}$$

In this context, K_2 (g mg^{-1} min^{-1}) corresponds to the equilibrium rate constant.

The most appropriate kinetic and isotherm models were determined using linear regression coefficient (R^2).

To assess the industrial applications of adsorbents, it is crucial to consider thermodynamic properties such as the change in entropy (ΔS), the change in enthalpy (ΔH), and the change in Gibbs free energy (ΔG). The standard change in Gibbs free energy (ΔG°) is a key thermodynamic parameter that elucidates the behavior of the adsorbent during adsorption. These thermodynamic parameters were calculated using the following eqs (eqs 10−12).

$$K_T = \frac{q_e}{C_e} \tag{10}$$

$$\ln K_T = \frac{\Delta S^\circ}{R} - \frac{\Delta H^\circ}{RT} \tag{11}$$

$$\Delta G^\circ = \Delta H^\circ - T\Delta S^\circ \tag{12}$$

In the above equations, T represents the temperature in Kelvin (K), R stands for the ideal gas constant, and K_T denotes the thermodynamic equilibrium constant.

2.5. Desorption Study. Regenerating the adsorbent plays a crucial role in rendering it a cost-effective and sustainable material for water treatment applications. During the recyclability test of the adsorbent, a specific quantity of PTh@Fe was introduced into 100 mL solutions containing 1 mg/L of As(III) and As(V). These solutions were then agitated for 24 h. Subsequently, the adsorbents were separated through filtration and subjected to drying in a vacuum oven at 60 °C for 12 h. The arsenic content in the filtrates was quantified using an atomic absorption spectrometer. To desorb the As(III) and As(V) loaded adsorbents, they were immersed in 100 mL of 0.1 M NaOH solution and agitated for 3 h at room temperature. The desorbed adsorbents underwent filtration, followed by multiple washes with water, and were finally dried in an oven for 3 h at 60 °C. This adsorption and desorption cycle was repeated five times, after which the arsenic content in the remaining solutions was determined.

3. RESULTS AND DISCUSSION

3.1. Characterization of the Adsorbent. *3.1.1. FTIR Study.* The FTIR spectra presented in Figure 2a depict the distinctive features of PTh, PTh@Fe, As(III) loaded PTh@Fe, and As(V) loaded PTh@Fe. In the spectrum of pure polythiophene (PTh), the peak at 3436 cm^{-1} corresponds to the O−H stretching vibration. Additionally, the peaks at 1115 and 1040 cm^{-1} can be attributed to C−H in-plane deformation, while the specific peak at 790 cm^{-1} corresponds to C−H out-of-plane deformation in polythiophene. Two

https://doi.org/10.1021/acsomega.4c03184
ACS Omega 2024, 9, 37012−37024

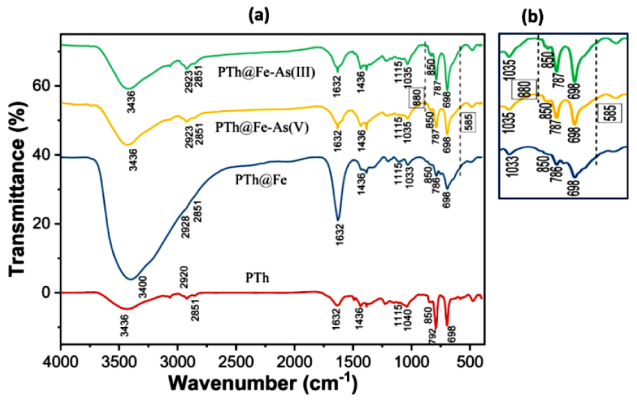

Figure 2. (a) The FTIR spectra of PTh, PTh@Fe, PTh@Fe treated with As(III), and PTh@Fe treated with As(V). (b) A close-up view of the peak in the FTIR spectra of PTh@Fe, PTh@Fe treated with As(III), and PTh@Fe treated with As(V).

other characteristic peaks at 1632 and 1436 cm^{-1} are ascribed to the C═C asymmetric and symmetric vibrations in the thiophene ring, respectively. Weak absorption bands around 850 cm^{-1} indicate the C−S stretching vibrations, and the peak at approximately 698 cm^{-1} is attributed to the C−S−C bending vibration. The peaks around 2920 and 2851 cm^{-1} correspond to the aromatic stretching and C−H alkene stretching, respectively.[36]

Comparatively, several peak wavenumbers and intensities show variations in PTh@Fe, As(III) loaded PTh@Fe, and As(V) loaded PTh@Fe compared to pure polythiophene. These changes are a consequence of the modification of PTh with Fe and alterations in bonding energies. In PTh@Fe, weak adsorption bands at 585 cm^{-1} may be attributed to the Fe−O stretching vibration of Fe_3O_4 and Fe_2O_3, indicating the incorporation of zerovalent iron (ZVI) particles into the PTh matrix. The shift of the O−H stretching peak from 3436 to 3400 cm^{-1} in PTh@Fe is due to a coordination reaction between 3d space orbitals and the lone pair of oxygen (O) atoms, resulting in a reduction in the bonding force constant and electron cloud density of the O−H group.[37] Notably, the characteristic peak at 3400 cm^{-1} shifts back to 3436 cm^{-1} after the adsorption of both As(III) and As(V), potentially indicating the transformation of ZVI particles on the surface to FeOOH.

3.1.2. Morphological and Compositional Study. The surface morphology of both untreated and treated PTh and PTh@Fe was analyzed using scanning electron microscopy, as illustrated in Figure 3. The SEM image of PTh (Figure 3a) reveals a granular morphology with random distribution. In contrast, the composite image (Figure 3b) shows the presence of spherical particles, indicating the loading of iron particles

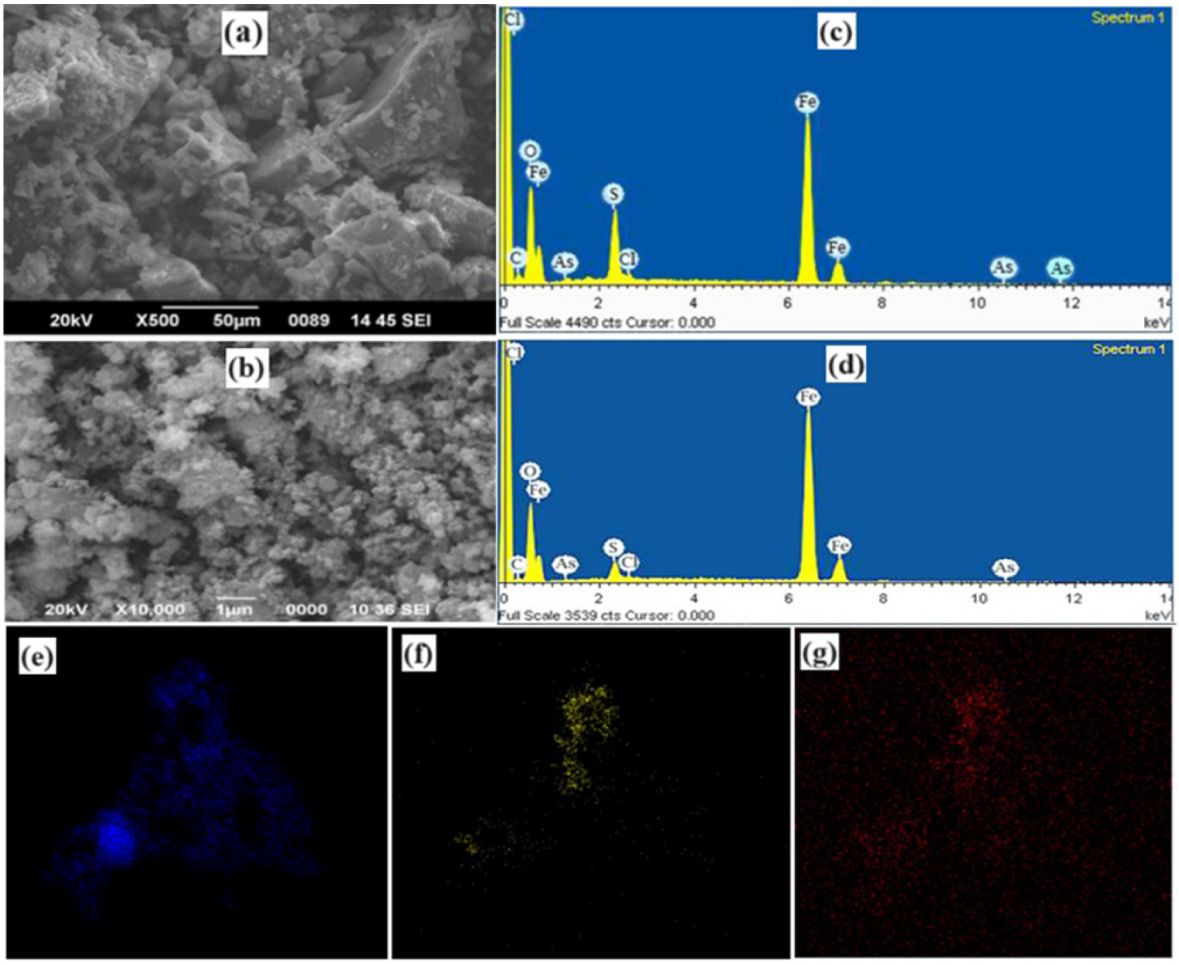

Figure 3. SEM image of (a) PTh, (b) PTh@Fe, along with the EDX, (c) As(III) treated and (d) As(V) treated PTh@Fe composite. EDX elemental mapping of (e) Fe, (f) S, and (g) C in PTh@Fe composite.

https://doi.org/10.1021/acsomega.4c03184
ACS Omega 2024, 9, 37012−37024

onto the surface of PTh. Remarkably, upon treatment with As(III) and As(V) (Supporting Information), there is no significant alteration in the composite's morphology.

The EDX spectrum of the composite (Supporting Information) reveals the presence of carbon (C) and sulfur (S), which aligns with polythiophene's composition. Additionally, the detection of iron (Fe) peaks in the spectrum provides evidence that iron has been effectively incorporated into the polythiophene matrix. Moreover, the presence of arsenic in the EDX spectrum (Figure 3c,d) confirms the successful adsorption of arsenic by the composite.

EDX elemental mapping of PTh@Fe revealed that Fe particles are uniformly distributed in the polymeric matrix (Figure 3e). From The EDX spectra and EDX surface mapping of PTh@Fe composite indicates the presence of Fe particles in the polymer matrix besides S and C originating from PTh as shown in Figure 3f,g respectively.

3.1.3. XRD Analysis. In the case of the PTh@Fe composite, diffraction peaks are observed at 2θ angles of 43.64° and 63.10°, corresponding to the (110) and (200) planes of zerovalent iron (ZVI), indicating a body-centered cubic structure,[19] as depicted in Figure 4. Conversely, in the case

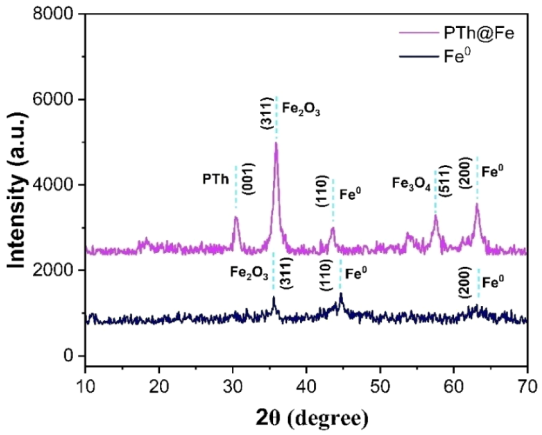

Figure 4. XRD pattern of zerovalent iron (ZVI) and PTh@Fe composite.

of pure ZVI, these peaks are observed at 2θ angles of 44.73° and 63.10°. Additionally, X-ray diffraction reveals peaks at 2θ angles of 35.55° and 35.95° for ZVI and PTh@Fe, respectively, which can be attributed to the (311) plane of Fe_2O_3 formed due to the oxidation of ZVI particles.[38,39] XRD pattern of PTh@Fe composite, the peak at 2θ of 57.51° corresponds to the (511) plane of Fe_3O_4 which was also formed due to the oxidation of ZVI particles.[40] This indicates that ZVI particles are enveloped by a layer of iron oxide.

Furthermore, the XRD pattern of polythiophene typically exhibits a peak at around 20°, indicating its amorphous nature, specifically the (001) plane.[41] However, in the PTh@Fe composite, a new peak emerges at 30.46° for polythiophene. This is attributed to the encapsulation of ZVI within the polythiophene macromolecule, resulting in a modification of the internal structure.[42] This confirms the successful incorporation of ZVI into the polythiophene macromolecular chain.

3.1.4. XPS Study. The XPS survey spectrum of the PTh@Fe composite reveals the presence of Fe 2p peaks, indicating the successful loading of ZVI particles onto the polymeric matrix. Figure 5b displays the Fe 2p core level spectrum, where deconvoluted peaks centered at 710.54 and 712.42 eV correspond to the binding energies of the Fe $2p_{3/2}$orbital.

The peak at 724.42 eV corresponds to the Fe $2p_{1/2}$ orbital in Fe_2O_3,[19] with an additional satellite peak appearing at a binding energy of 719.11 eV. These peaks provide confirmation that the loaded ZVI particles on the PTh matrix are enveloped by a layer of iron oxide.[43] Notably, there is no observed peak around 706 eV for Fe $2p_{1/2}$, which is characteristic of pure Fe. This observation suggests that the layer of iron oxides surrounding the ZVI particles is thicker than 10 nm, as XPS can only detect photoelectrons from the outer surface within this range.

3.2. Result of Batch Experiment. *3.2.1. Impact of Adsorbent Dosage.* The quantity of adsorbent dosage is a crucial parameter, as it determines the extent of heavy metal adsorption onto the adsorbent material. In this batch experiment, different amounts of adsorbent (0.05, 0.1, 0.3, 0.7, and 1 g/L) were introduced into Erlenmeyer flasks containing 100 mL of 1 mg/L of As(III) and As(V) solution separately. To standardize the pH of the arsenic solutions, adjustments were made using 0.1 M NaOH and 0.1 M HCl solutions. Subsequently, these solutions were agitated in an orbital shaker for a duration of 24 h at 30 °C. This entire batch experiment was replicated three times, and the mean percentage removal value was recorded. A graphical representation of adsorbent dose versus percentage removal, with standard deviation as error bars, was generated.

From Figure 6a, it is evident that as the adsorbent dose increases from 0.05 to 1 g/L, the percentage uptake of both As(III) and As(V) also increases. This behavior can be attributed to the greater availability of binding sites for adsorption. Specifically, for As(III), the maximum percentage removal was determined to be 98.7%, while for As(V), it reached 98.8% at the adsorbent dose of 1 g/L. Notably, the percentage removal exhibits only a marginal increase from 0.3 g/L to 1 g/L for both As(III) and As(V).Consequently, 0.3 g/L has been identified as the optimal dosage for further batch experiments.

3.2.2. Effect of pH. To investigate the impact of pH on arsenic uptake by the PTh@Fe composite, the pH levels of the arsenic solutions were adjusted within the range of 3 to 11. Each solution maintained a constant adsorbent dose (0.3 g/L), initial arsenic concentration (1 mg/L), temperature (30 °C), and contact time (24 h). To enhance accuracy, each experiment was conducted in triplicate. As depicted in Figure 6b, it becomes evident that the percentage removal decreases as the pH of the solution increases. The point of zero charge of the adsorbent is determined to be at pH = 6.11 as evident from the Supporting Information. For both As(III) and As(V), complete removal (100%) was observed at pH 3. The adsorbent demonstrated efficient arsenic removal capabilities within the acidic to neutral pH range. This phenomenon can be attributed to the presence of negatively charged arsenic species, such as $H_2AsO_4^-$ and $HAsO_4^{2-}$, which are attracted to the positively charged surface of the PTh@Fe composite. Conversely, at pH levels exceeding 7, the surface of the composite acquires an overall negative charge, resulting in the repulsion of negatively charged arsenic species. This repulsion causes a decline in the percentage removal. Furthermore, at pH levels exceeding 9.2, the neutral species (H_3AsO_3) of As(III) dissociates into negatively charged species, which are also

https://doi.org/10.1021/acsomega.4c03184
ACS Omega 2024, 9, 37012−37024

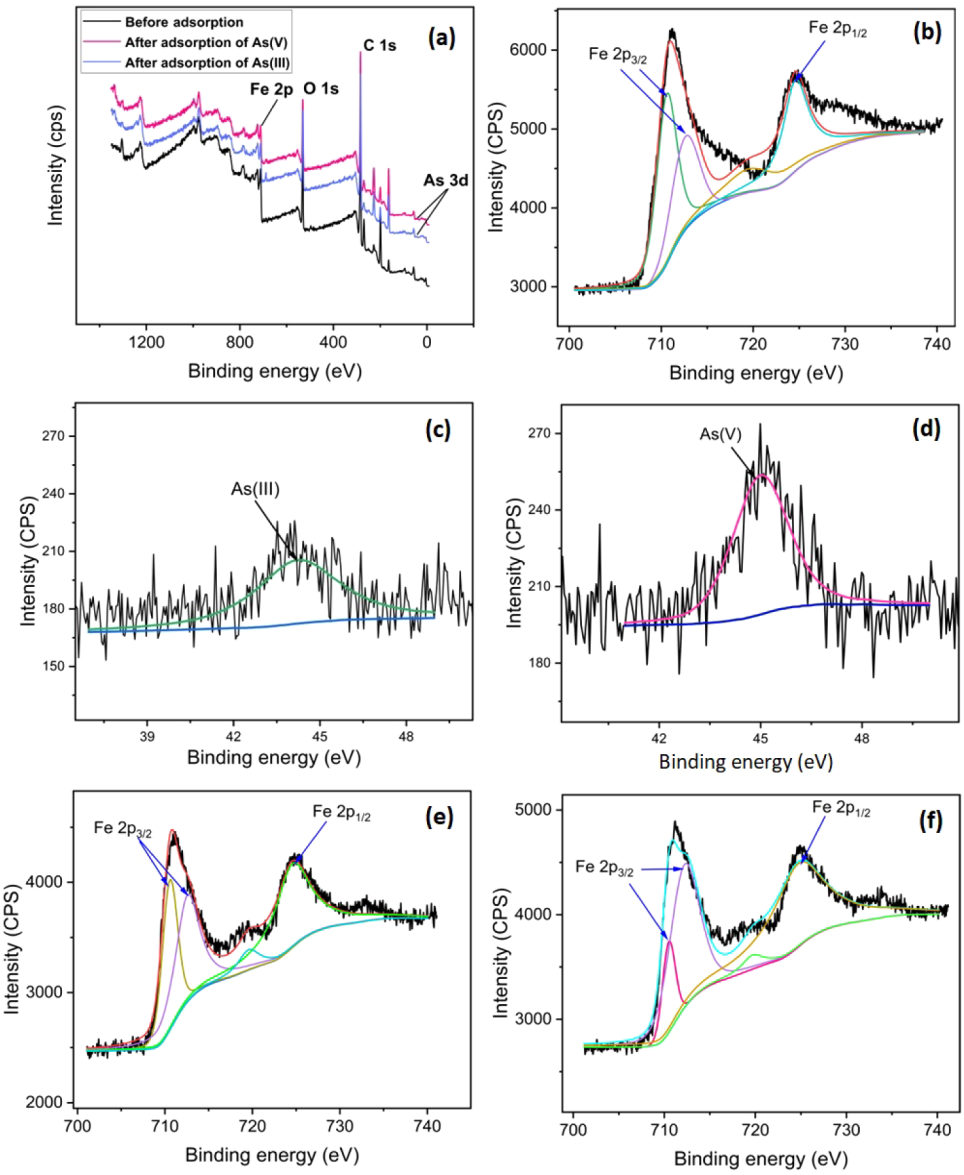

Figure 5. (a) XPS survey spectrum of PTh@Fe, (b) XPS spectrum of Fe 2p, (c) XPS spectrum of As 3d after adsorption of As(III), and (d) XPS spectrum of As 3d after adsorption of As(V), and (e) Fe 2p spectrum after adsorption of As(III) and (f) Fe 2p spectrum after adsorption of As(V).

repelled by the negatively charged adsorbent. This dissociation contributes to a reduction in the percentage removal.

3.2.3. Effect of Initial Arsenic Concentration. To investigate the impact of initial arsenic concentration on arsenic uptake by the PTh@Fe composite, varying concentrations of arsenic solutions (ranging from 0.1 to 5 mg/L) were prepared in separate Erlenmeyer flasks. The adsorbent dosage (0.3 g/L), contact time (24 h), solution pH (7), and temperature (30 °C) remained constant throughout the experiments. This batch experiment was conducted in triplicate, and the mean percentage removal values were considered for analysis. As illustrated in Figure 6c, it becomes evident that the percentage removal gradually decreases with an increase in the initial arsenic concentration. This decline can be attributed to the saturation of binding sites as the adsorption process progresses. Both As(III) and As(V) species exhibit a reduction in percentage removal as the initial arsenic concentration rises. Remarkably, the adsorbent demonstrates the capability to completely remove As(V) and even the more toxic As(III) species when the initial arsenic concentrations are as low as 0.1 and 0.3 mg/L.

3.2.4. Impact of Contact Time. The contact time between the arsenic solution and the adsorbent is a critical factor as it directly impacts the efficiency and feasibility of implementing the process at the pilot scale. To evaluate the influence of exposure time on arsenic adsorption, a batch experiment was conducted at various time intervals (60, 180, 360, 720, and 1440 min). Throughout this experiment, other parameters such as adsorbent dosage (0.3 g/L), arsenic concentration (1 mg/L), solution pH (7), and temperature (30 °C) were maintained at constant levels. This batch experiment was performed in triplicate for accuracy. As illustrated in Figure 6d, it is evident that the percentage removal for both arsenic species increases with prolonged exposure time. The maximum adsorption was achieved at 2880 min (48 h), with 95.83% removal for As(III) and 96.4% removal for As(V). Notably, there is a steep increase in percentage removal from 60 to 1440 min for both As(III) and As(V). For As(III), the percentage

https://doi.org/10.1021/acsomega.4c03184
ACS Omega 2024, 9, 37012−37024

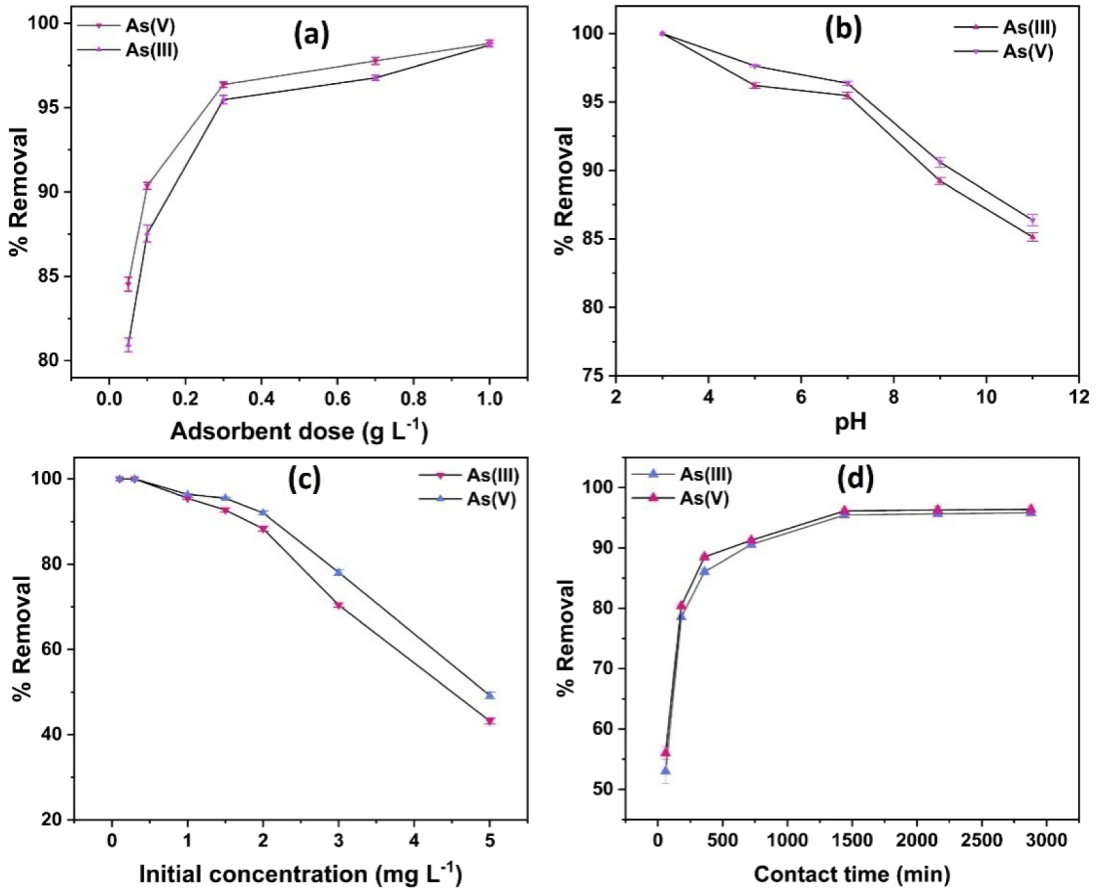

Figure 6. Influence of various factors on arsenic uptake by the PTh@Fe composite: (a) The effect of adsorbent dosage, (b) The effect of pH, (c) The effect of initial arsenic concentration and (d) The effect of contact time.

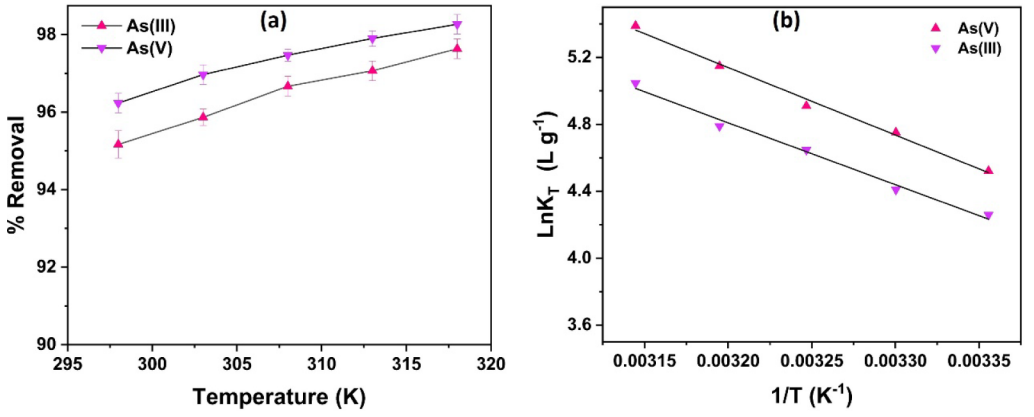

Figure 7. (a) Impact of temperature and (b)Vant Hoff's plot for arsenic removal.

removal increases from 53% to 95.47%, while for As(V), it increases from 56% to 96.13%. However, after this point (1440 min), no noticeable change in percentage removal is observed, likely due to the saturation of adsorption sites. Therefore, 1440 min can be considered as adsorption equilibrium time.

3.2.5. Thermodynamic Study. To investigate the impact of temperature, a batch experiment was conducted at different temperatures: 298, 303, 308, 313, and 318 K. Throughout the adsorption process, other parameters such as adsorbent dosage (0.3 g/L), initial concentration (1 mg/L), contact time (24 h), solution pH (7), and temperature (30 °C) were maintained at constant levels. It was observed that, with the increase in the temperature the percentage removal for both the arsenic species increases. For As(III), the percentage removal increased from 95% to 97%, while for As(V), it increased from 96% to 98% as shown in Figure 7a.

The thermodynamic parameters for arsenic adsorption by the PTh@Fe composite, calculated from Vant Hoff's plot (Figure 7b), and detailed are provided in the Supporting Information. The Van't Hoff plot and the corresponding thermodynamic data for all the replicated experiments are presented and explained in the Supporting Information. Notably, the positive value of ΔH suggests that the adsorption occurs via an endothermic process, indicating that an increase

https://doi.org/10.1021/acsomega.4c03184
ACS Omega 2024, 9, 37012−37024

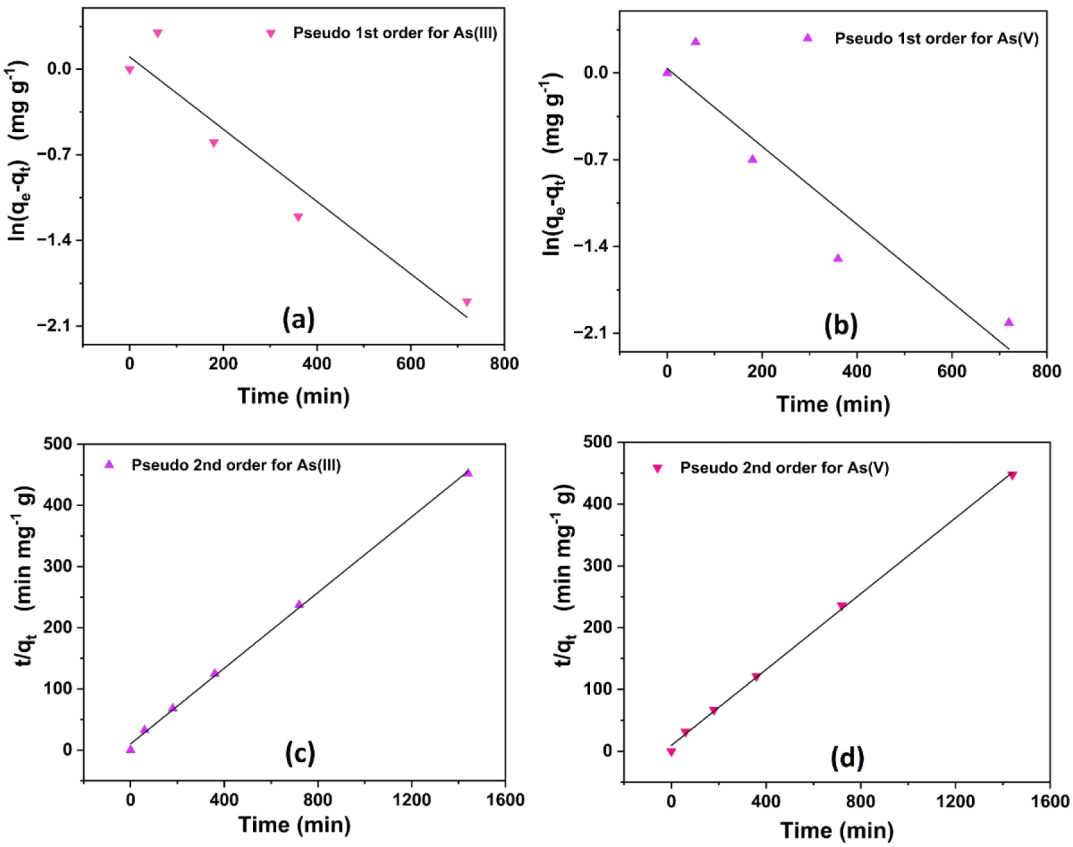

Figure 8. Application of the pseudo1st-order kinetic model to depict (a) As(III) uptake and (b) As(V) uptake, as well as the pseudo2nd-order kinetic model for (c) As(III) uptake and (d) As(V) uptake.

in temperature is favorable for arsenic adsorption by the composite. Furthermore, the positive value of ΔS indicates that arsenic uptake on the composite increases the randomness at the solid−liquid interface.[44] Importantly, at all experimental temperatures, the values of ΔG were found to be negative, implying the feasible and spontaneous nature of arsenic adsorption on the composite.

3.2.6. Adsorption Kinetics. Adsorption kinetics plays a pivotal role in water purification processes. It essentially delineates the dynamics of interaction between the adsorbent and adsorbate within an aqueous system.[45] Understanding the kinetics of adsorption is instrumental in determining the necessary retention time for the completion of the adsorption process, which hinges on the rate of solute adsorption. To ascertain kinetic parameters, we employed pseudo 1st-order and pseudo 2nd-order models. The batch experiment encompassed various time intervals (1, 3, 6, 12, and 24 h), with all other variables held constant. The experimental data points up to 750 min were used for the pseudo-first-order kinetic model, whereas all data points up to 1440 min were used for the pseudo-second-order model. This discrepancy arises because the $\log(q_e - q_t)$ value cannot be determined at t = 1440 min, as $(q_e - q_t)$ equals zero. Therefore, we fitted the pseudo-first-order model only up to 750 min. As illustrated in Figure 8, we fitted these two aforementioned isotherm models for the adsorption of As(III) and As(V) by the adsorbent, and the corresponding kinetic parameters are presented in Supporting Information along with similar data obtained from replication experiments. Model fitting for the replication experiments for kinetic study is also presented and explained in the Supporting Information. It was found that the pseudo2nd-order model is a better fit for both As(V) and As(III) adsorption, exhibiting higher correlation coefficients. Specifically, the correlation coefficient (R^2) for As(III) is 0.9985, while for As(V), it stands at 0.9986 in the pseudo 2nd-order model. While for pseudo1st-order model the value of R^2 for As(III) and As(V) are 0.8934 and 0.8565 respectively. Notably, the value of q_e obtained from the pseudo 2nd-order model closely approximates the experimental q_e value for both As(III) and As(V) uptake. These outcomes strongly suggest that the adsorption of arsenic species onto the PTh@Fe composite occurs through a chemisorption mechanism.

3.2.7. Adsorption Isotherm. Equilibrium adsorption isotherm data are crucial for the effective design and operation of adsorption systems, providing insights into the interaction between adsorbate and adsorbent. Two widely used adsorption isotherm models, namely the (1) Langmuir and (2) Freundlich adsorption isotherm models, were employed in this study. The linearized plots for both Langmuir (1) and Freundlich (2) adsorption isotherms are presented in Figure 9a,b, and the corresponding adsorption isotherm data extracted from these plots are presented in the Supporting Information along with data of replication experiments. Model fitting of all the replication experiments is also presented in the Supporting Information. Comparing the two models, the Langmuir model demonstrates a closer fit to the isotherm data, as indicated by its higher correlation coefficients (R^2). The maximum adsorption capacities (q_{max}) determined from the linearized Langmuir plot are 8.62 mg/g for As(V) uptake and 7.57 mg/g for As(III) uptake, respectively. These results highlight that the

https://doi.org/10.1021/acsomega.4c03184
ACS Omega 2024, 9, 37012−37024

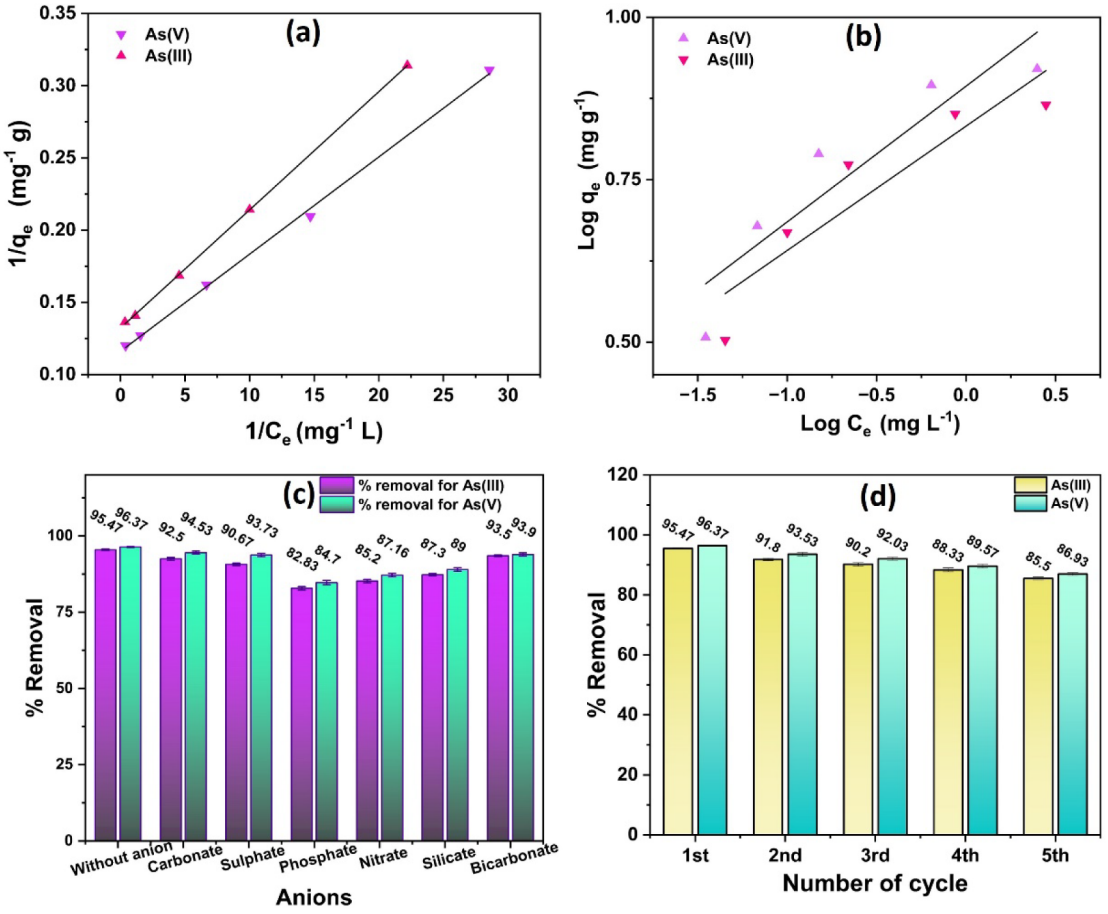

Figure 9. Linearized plots for (a) Langmuir adsorption isotherm model, and (b) Freundlich adsorption isotherm model, illustrating the adsorption of arsenite [As(III)] and arsenate [As(V)]; (c) the impact of coexisting anions, and (d) the reusability of the PTh@Fe composite for arsenic adsorption.

adsorption capacities of PTh@Fe are superior to those of pure polythiophene. The Langmuir model suggests a single-layer adsorption of arsenic species on the adsorbent surface.

3.2.8. Effect of Coexisting Anions. Various substances can be found in natural water systems, and the presence of different anions can influence how effectively arsenate and arsenite are adsorbed onto the adsorbent. Therefore, certain anions, namely CO_3^{2-}, SO_4^{2-}, PO_4^{3-}, HCO_3^{-}, SiO_3^{2-}, and NO_3^{-}were selected to investigate their impact on the arsenic adsorption capacity of the adsorbent. The batch experiment was conducted using an anion concentration of 0.5 mg/L in the arsenic solution, while keeping the other parameters constant, including adsorbent dose (0.3 g/L), initial arsenic concentration (1 mg/L), pH of the solution (7), contact time (24 h), and temperature (30 °C). Each batch experiment was repeated three times. As illustrated in Figure 9c, it is evident that CO_3^{2-}, SO_4^{2-}, and HCO_3^{2-} ions do not significantly impact arsenic adsorption on the composite. However, PO_4^{3-}, SiO_3^{2-}, and NO_3^{-} ions notably affect arsenic adsorption by the adsorbent. In the case of As(III) removal, the percentage uptake decreases from 95.47% to 82.83%, 87.3%, and 85.2% due to the presence of PO_4^{3-}, SiO_3^{2-}, and NO_3^{-} respectively. Similarly, for As(V), the percentage uptake decreases from 96.37% to 84.7%, 89% and 87.16% due to the presence of PO_4^{3-}, SiO_3^{2-}, and NO_3^{-} ions. This reduction in As(III) and As(V) removal in the presence of PO_4^{3-} and NO_3^{-} is due to the competitive interaction with As(III) and As(V). Moreover, SiO_3^{2-} and PO_4^{3-} ions exhibit structural similarities with arsenic species, forming inner-sphere complexes with hydroxyl groups present at the surface of the adsorbent. Hence, the reduction in arsenic removal due to the presence of PO_4^{3-}, SiO_3^{2-}, and NO_3^{-} ions may be attributed to their competition with the arsenic species for the adsorption sites.

3.2.9. Reusability. The recyclability and reusability of the employed adsorbent material are critical factors to consider when evaluating cost-effectiveness. The reusability test was conducted using 0.3 g/L of the adsorbent in a 1 mg/L arsenic solution, subjected to 24 h of treatment at 30 °C. The pH of the solution was maintained at 7 during the adsorption process. As shown in Figure 9d, the percentage removal gradually decreases when the adsorption−desorption cycle is repeated five times. For As(III), the percentage removal decreases from 95.47% to 85.5% over the course of five cycles, and for As(V), the percentage removal drops from 96.37% to 86.93% during the same cycle repetitions. Based on the results obtained, it can be concluded that PTh@Fe exhibits considerable reusability in removing arsenic from contaminated water.

3.3. Mechanism of Arsenic Adsorption. The PTh@Fe composite, comprising polythiophene and iron particles (Fe, Fe_2O_3, Fe_3O_4), effectively removes arsenic through a synergistic effect. The FTIR spectra of PTh@Fe composites (Figure 2a,b) treated with As(III) and As(V) show a new peak at 880 cm^{-1}, which corresponds to the As−O stretching

https://doi.org/10.1021/acsomega.4c03184
ACS Omega 2024, 9, 37012−37024

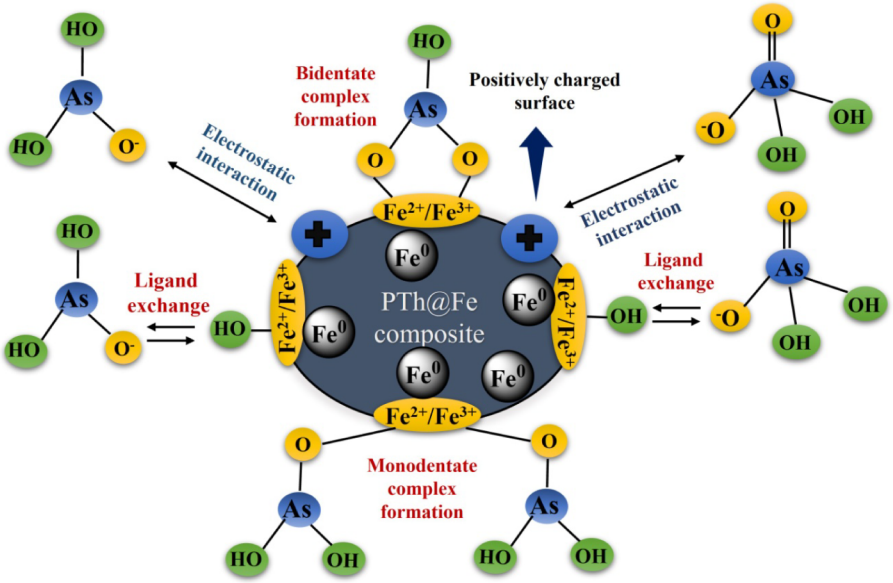

Figure 10. Plausible mechanism of arsenic adsorption on PTh@Fe composite.

vibration. This indicates the formation of a Fe−As complex on the adsorbent surface.[26] Akoto et al. have described that the adsorption of As(III) and As(V) involves the formation of monodentate and bidentate complexes in a composite made of magnetite and zerovalent iron stabilized with polyethylenimine.[46]

The survey spectrum shows (Figure 5a), As 3d core level peaks, confirming arsenic adsorption onto the PTh@Fe composite. Specifically, As(III) treated composites show a peak at 44.1 eV, and As(V) treated composites show a peak at 45.09 eV, corresponding to the binding energy of As 3d (Figure 5c,d).

Within the PTh@Fe composite, ZVI reacts with dissolved oxygen and water, producing Fe^{3+} and Fe^{2+} ions. These ions, influenced by redox potential and pH, form various iron hydroxides, oxides, and oxyhydroxides. This formation is evident from the Fe 2p core level peaks, with Fe $2p_{3/2}$ peaks at 710 and 712 eV, and a Fe $2p_{1/2}$ peak at 724 eV, indicating the oxidized form of Fe (III) (Figure 5e,f). This transformation replaces surface-bonded OH ligands with arsenate and arsenite ions, allowing these species to adsorb onto the newly formed oxides and hydroxides. This is also evident in the FTIR spectra (Figure 2a), where the intensity of the −OH peak significantly decreases after arsenic adsorption by the composite compared to the pure PTh@Fe composite. This indicates that −OH groups are involved in the adsorption process.

Electrostatic interactions play a significant role in arsenic removal. At a pH below 6.11 (ZPC), the composite becomes positively charged and binds to the negatively charged arsenic species. As our previous research indicates, polythiophene also interacts with arsenic, enhancing the composite's effectiveness for arsenic adsorption.[35] Chloride ions in the polymer chain may exchange with the negatively charged arsenic species. These arsenic species bind to the positively charged surface of polythiophene through sulfur−oxygen linkages. Additionally, weak van der Waals interactions occur between the hydrogen atoms of polythiophene and the oxygen atoms of arsenic species. The plausible mechanism of arsenic adsorption by PTh@Fe composite is demonstrated in Figure 10.

3.4. DFT. To confirm the suggested mechanism for arsenic adsorption, an additional study was carried out using the software package Gaussian Atomic and Molecular Structure system (GAMESS version 2022 R2), employing density functional theory (DFT) calculations.[47,48] The optimization of the ground state geometry employed Kohn−Sham density functional theory, utilizing the B3LYP hybrid density exchange functional and the 6-311G basis set. This particular function utilized in the adiabatic connection method includes fractions of the exact Hartree−Fock exchange energy, which are computed based on the Kohn−Sham molecular orbitals. Furthermore, stationary points were subsequently identified by calculating vibrational frequencies, without considering dispersion effects, within the same theoretical framework.

Figure 11 shows the optimized structures of Fe in zerovalent form, +2 state and +3 state with adsorption of arsenite and arsenate molecules. According to the data provided in the Supporting Information, iron in all its forms (ZVI, +2, or +3) functions as an effective adsorption agent for both As(III) and As(V). Based on the ground state energy values, it is evident that the most stable adsorption reaction occurs with the Fe(+3) form of iron, followed by the zerovalent form, for both arsenite and arsenate. Notably, the energies of the highest occupied molecular orbital (HOMO) and lowest unoccupied molecular orbital (LUMO) are established quantum mechanical descriptors with a substantial influence on various chemical interactions. Meanwhile, the frontier molecular orbital (FMO) offers valuable insights into the reactivity of a molecule, and the spatial distribution of the frontier orbital can effectively depict the location of the active site. The compositions of the HOMO and LUMO frontier orbitals as calculated using the density functional theory (DFT) with a 6-311G orbital energy level. The HOMO energy indicates the electron's capacity to donate, whereas the LUMO energy signifies the electron's ability to accept. The energy gap between these orbitals characterizes the chemical reactivity and kinetic stability of the molecules. A larger HOMO−LUMO energy gap signifies higher kinetic energy and increased chemical reactivity. The close proximity of the HOMO and LUMO energy levels facilitates beneficial intramolecular charge transfer. The

https://doi.org/10.1021/acsomega.4c03184
ACS Omega 2024, 9, 37012−37024

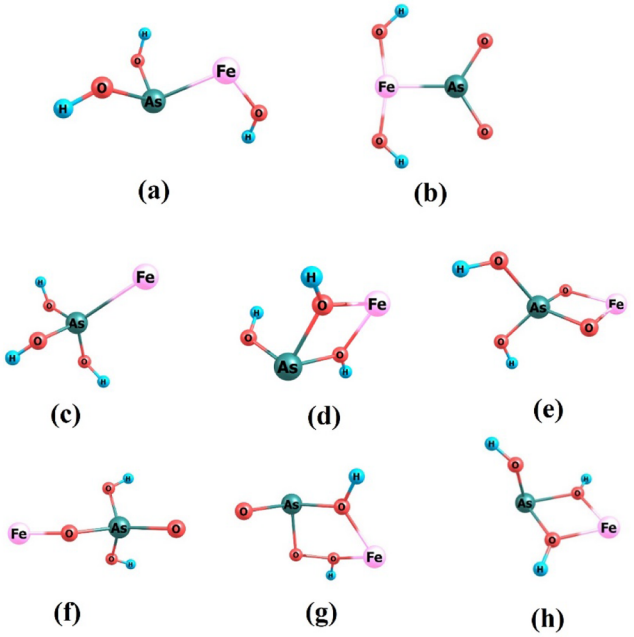

Figure 11. Ground state optimized structure of (a) ZVI+arsenite, (b) ZVI+arsenate, (c,d) Fe(+2)+arsenite, (e,f) Fe(+2)+arsenate, (g) Fe(+3)+arsenite, and (h) Fe(+3)+arsenate.

computational analysis presented here serves to validate the findings of the experimental study. Furthermore, it offers a logical basis for the physical interpretation of the observed phenomena.

4. CONCLUSION

In conclusion, this study has demonstrated the potential of iron-functionalized polythiophene (PTh@Fe) as an effective adsorbent for removing both As(III) and As(V) from aqueous solutions. The synthesized PTh@Fe composite was thoroughly characterized using FTIR, SEM-EDX, XRD, and XPS, revealing the successful loading of iron particles onto the PTh matrix and providing insights into the arsenic adsorption mechanism. Batch experiments were conducted to evaluate the effects of adsorbent dosage, pH, initial arsenic concentration, and contact time on arsenic removal. Results showed that increased adsorbent dosages and longer contact times enhanced arsenic removal efficiency, with optimal performance under acidic to neutral pH conditions and decreased efficiency at higher pH levels. Higher initial arsenic concentrations led to reduced removal percentages, indicating adsorption site saturation. Thermodynamic analysis indicated that the adsorption process was endothermic, spontaneous, and involved increased entropy at the solid−liquid interface, while kinetic studies suggested a pseudo-second-order mechanism, implying chemisorption as the predominant process. Adsorption isotherm modeling showed that the Langmuir model best fit the experimental data, with maximum adsorption capacities of 8.62 mg/g for As(V) and 7.57 mg/g for As(III). Coexisting anions such as carbonate and sulfate had minimal impact on arsenic adsorption, whereas phosphate ions competed for adsorption sites. The PTh@Fe composite exhibited good reusability, highlighting its promise for practical applications in arsenic-contaminated water remediation. Additionally, Density Functional Theory (DFT) calculations provided theoretical support for the feasibility of arsenic adsorption onto iron species in various oxidation states.

This study thoroughly explored the synthesis, characterization, and effectiveness of the PTh@Fe composite for arsenic removal. The results highlight its potential as an efficient and sustainable solution for addressing arsenic contamination, which can significantly improve public health and environmental quality. These findings open the door for future research and practical applications of this promising technology.

■ ASSOCIATED CONTENT

Supporting Information

The Supporting Information is available free of charge at https://pubs.acs.org/doi/10.1021/acsomega.4c03184.

1 SEM-EDX study; thermodynamic study; study of adsorption isotherm; study of kinetics; DFT study; removal rates of As(III) and As(V) for various adsorbent doses; determination of zero point charge of the adsorbent; raw data for model fitting (PDF)

■ AUTHOR INFORMATION

Corresponding Authors

Surajit Konwer − *Department of Chemistry, Dibrugarh University, Dibrugarh 786004, India;* orcid.org/0000-0002-8878-7076; Email: surajitkonwer@dibru.ac.in

Ankur Gogoi − *Department of Physics, JB College, Jorhat, Assam 785001, India*; Email: ankurgogoi@gmail.com

Authors

Rupkamal Chetia − *Department of Chemistry, Dibrugarh University, Dibrugarh 786004, India*

Shrutipriya Devi − *Department of Chemistry, Dibrugarh University, Dibrugarh 786004, India*

Nishant Shukla − *Department of Physics, The Assam Kaziranga University, Jorhat, Assam 785006, India*

Abhishek Hazarika − *Coal & Energy Division, CSIR − North East Institute of Science and Technology (NEIST), Jorhat, Assam 785006, India*

Shreemoyee Bordoloi − *Department of Chemistry, MDKG College, Dibrugarh, Assam 786001, India*

Binod Pokhrel − *Department of Chemical Sciences, Tezpur University, Tezpur, Assam 784028, India*

Binoy K Saikia − *Coal & Energy Division, CSIR − North East Institute of Science and Technology (NEIST), Jorhat, Assam 785006, India;* orcid.org/0000-0002-3382-6218

Complete contact information is available at: https://pubs.acs.org/10.1021/acsomega.4c03184

Author Contributions

This research has seen significant contributions from all authors, each playing a distinct role; R.C. conducted the synthesis, characterization, and analysis of the composite, and authored the manuscript. S.D. conducted the synthesis, characterized the samples, and evaluated their properties. N.S. performed DFT calculations and contributed to the theoretical investigation. A.H. conducted characterizations and property evaluations of the samples. S.B. conducted water analysis and contributed to writing, review, and editing. B.P. executed batch experiments for water treatment using the adsorbent. B.K.S. conducted characterization, property evaluations, and contributed to review and editing. A.G. carried out

https://doi.org/10.1021/acsomega.4c03184
ACS Omega 2024, 9, 37012−37024

DFT calculations and provided supervision for the theoretical investigation. S.K. provided overall supervision and guidance throughout the research process.

Notes

The authors declare no competing financial interest.

■ ACKNOWLEDGMENTS

The authors thank Dibrugarh University for providing all the infrastructural facility. We acknowledge the Department of Science and Technology for financial assistance under DST-FIST programme, DST-PURSE programme [no. SR/PURSE/2022/143(C)] and the UGC, New Delhi for the Special Assistance Programme (UGC-SAP) to the Department of Chemistry, Dibrugarh University.

■ ABBREVIATIONS

PTh, polythiophene; PTh@Fe, iron-functionalized polythiophene; As, arsenic; DFT, density functional theory

■ REFERENCES

(1) Joshi, S.; Sharma, M.; Kumari, A.; Shrestha, S.; Shrestha, B. Arsenic removal from water by adsorption onto iron oxide/nanoporous carbon magnetic composite. *Appl. Sci.* **2019**, *9* (18), 3732.

(2) Wang, Y.; Yu, J.; Wang, Z.; Liu, Y.; Zhao, Y. A review on arsenic removal from coal combustion: advances, challenges and opportunities. *Chem. Eng. J.* **2021**, *414*, 128785.

(3) Vadahanambi, S.; Lee, S. H.; Kim, W. J.; Oh, I. K. Arsenic removal from contaminated water using three-dimensional graphene-carbon nanotube-iron oxide nanostructures. *Environ. Sci. Technol.* **2013**, *47* (18), 10510−10517.

(4) Muñiz, G.; Fierro, V.; Celzard, A.; Furdin, G.; Gonzalez-Sánchez, G.; Ballinas, M. L. Synthesis, characterization and performance in arsenic removal of iron-doped activated carbons prepared by impregnation with Fe (III) and Fe (II). *J. Hazard. Mater.* **2009**, *165* (1−3), 893−902.

(5) Chandra, V.; Park, J.; Chun, Y.; Lee, J. W.; Hwang, I. C.; Kim, K. S. Water-dispersible magnetite-reduced graphene oxide composites for arsenic removal. *ACS Nano* **2010**, *4* (7), 3979−3986.

(6) Assaad, N.; Sabeh, G.; Hmadeh, M. Defect control in Zr-based metal−organic framework nanoparticles for arsenic removal from water. *ACS Appl. Nano Mater.* **2020**, *3* (9), 8997−9008.

(7) Tan, S. N.; Yong, J. W.; Ng, Y. F. Arsenic exposure from drinking water and mortality in Bangladesh. *Lancet* **2010**, *376* (9753), 1641−1642.

(8) Luo, J.; Luo, X.; Hu, C.; Crittenden, J. C.; Qu, J. Zirconia (ZrO_2) embedded in carbon nanowires via electrospinning for efficient arsenic removal from water combined with DFT studies. *ACS Appl. Mater. Interfaces* **2016**, *8* (29), 18912−18921.

(9) Hong, Y.-S.; Song, K.-H.; Chung, J.-Y. Health effects of chronic arsenic exposure. *J Prev Med Public Health* **2014**, *47* (5), 245−252.

(10) Setyono, D.; Valiyaveettil, S. Chemically modified sawdust as renewable adsorbent for arsenic removal from water. *ACS Sustainable Chem. Eng.* **2014**, *2* (12), 2722−2729.

(11) Gu, Z.; Fang, J.; Deng, B. Preparation and evaluation of GAC-based iron-containing adsorbents for arsenic removal. *Environ. Sci. Technol.* **2005**, *39* (10), 3833−3843.

(12) Hao, L.; Liu, M.; Wang, N.; Li, G. A critical review on arsenic removal from water using iron-based adsorbents. *RSC Adv.* **2018**, *8* (69), 39545−39560.

(13) Escudero, C.; Fiol, N.; Villaescusa, I.; Bollinger, J. C. Arsenic removal by a waste metal (hydr) oxide entrapped into calcium alginate beads. *J. Hazard. Mater.* **2009**, *164* (2−3), 533−554.

(14) Ge, X.; Ma, Y.; Song, X.; Wang, G.; Zhang, H.; Zhang, Y.; Zhao, H. *β*-FeOOH nanorods/carbon foam-based hierarchically porous monolith for highly effective arsenic removal. *ACS Appl. Mater. Interfaces* **2017**, *9* (15), 13480−13490.

(15) Cao, A. M.; Monnell, J. D.; Matranga, C.; Wu, J. M.; Cao, L. L.; Gao, D. Hierarchical nanostructured copper oxide and its application in arsenic removal. *J. Phys. Chem. C* **2007**, *111* (50), 18624−18628.

(16) Clancy, T. M.; Hayes, K. F.; Raskin, L. Arsenic waste management: a critical review of testing and disposal of arsenic-bearing solid wastes generated during arsenic removal from drinking water. *Environ. Sci. Technol.* **2013**, *47* (19), 10799−10812.

(17) Hussam, A.; Munir, A. K. A simple and effective arsenic filter based on composite iron matrix: Development and deployment studies for groundwater of Bangladesh. *J. Environ. Sci. Health, Part A* **2007**, *42* (12), 1869−1878.

(18) Li, Z.; Wang, L.; Meng, J.; Liu, X.; Xu, J.; Wang, F.; Brookes, P. Zeolite-supported nanoscale zero-valent iron: New findings on simultaneous adsorption of Cd (II), Pb (II), and As (III) in aqueous solution and soil. *J. Hazard. Mater.* **2018**, *344*, 1−11.

(19) Bhaumik, M.; Noubactep, C.; Gupta, V. K.; McCrindle, R. I.; Maity, A. Polyaniline/Fe0 composite nanofibers: An excellent adsorbent for the removal of arsenic from aqueous solutions. *Chem. Eng. J.* **2015**, *271*, 135−146.

(20) Tarekegn, M. M.; Hiruy, A. M.; Dekebo, A. H. Nano zero valent iron (nZVI) particles for the removal of heavy metals (Cd^{2+}, Cu^{2+} and Pb^{2+}) from aqueous solutions. *RSC Adv.* **2021**, *11* (30), 18539−18551.

(21) Liu, K.; Li, F.; Cui, J.; Yang, S.; Fang, L. Simultaneous removal of Cd (II) and As (III) by graphene-like biochar-supported zero-valent iron from irrigation waters under aerobic conditions: Synergistic effects and mechanisms. *J. Hazard. Mater.* **2020**, *395*, 122623.

(22) Liu, X.; Lai, D.; Wang, Y. Performance of Pb (II) removal by an activated carbon supported nanoscale zero-valent iron composite at ultralow iron content. *J. Hazard. Mater.* **2019**, *361*, 37−48.

(23) Bordoloi, S.; Chetia, R.; Borah, G.; Konwer, S. Removal of As (III) and As (V) from water using reduced GO-Fe0 filled PANI composite. *J App Water Eng. Res.* **2022**, *10* (2), 117−128.

(24) Horzum, N.; Demir, M. M.; Nairat, M.; Shahwan, T. Chitosan fiber-supported zero-valent iron nanoparticles as a novel sorbent for sequestration of inorganic arsenic. *RSC Adv.* **2013**, *3* (21), 7828−7837.

(25) Jang, M.; Chen, W.; Cannon, F. S. Preloading hydrous ferric oxide into granular activated carbon for arsenic removal. *Environ. Sci. Technol.* **2008**, *42* (9), 3369−3374.

(26) Xu, L.; Shu, Z.; Feng, L.; Zhou, J.; Li, T.; Zhao, Z.; Wang, W. Fresh biomass derived biochar with high-load zero-valent iron prepared in one step for efficient arsenic removal. *J. Cleaner Prod.* **2022**, *352*, 131616.

(27) Joshi, N. C.; Malik, S.; Gururani, P. Utilization of polypyrrole/ZnO nanocomposite in the adsorptive removal of Cu^{2+}, Pb^{2+} and Cd^{2+} ions from wastewater. *Lett. Appl. NanoBiosci.* **2021**, *10* (3), 2339−2351.

(28) Rong, Y.; Yan, W.; Wang, Z.; Hao, X.; Guan, G. An electroactive montmorillonite/polypyrrole ion exchange film: Ultra-high uptake capacity and ion selectivity for rapid removal of lead ions. *J. Hazard. Mater.* **2022**, *437*, 129366.

(29) Karthik, R.; Meenakshi, S. Removal of Pb (II) and Cd (II) ions from aqueous solution using polyaniline grafted chitosan. *Chem. Eng. J.* **2015**, *263*, 168−177.

(30) Eisazadeh, A.; Eisazadeh, H.; Kassim, K. A. Removal of Pb (II) using polyaniline composites and iron oxide coated natural sand and clay from aqueous solution. *Synth. Met.* **2013**, *171*, 56−61.

(31) Karimi, Z.; Khalili, R.; Ali Zazouli, M. Surface modified polythiophene/Al_2O_3 and polyaniline/Al_2O_3 nanocomposites using poly (vinyl alcohol) for the removal of heavy metal ions from water: kinetics, thermodynamic and isotherm studies. *Water Sci. Technol.* **2021**, *84* (1), 182−199.

(32) Chen, J.; Dong, R.; Chen, S.; Tang, D.; Lou, X.; Ye, C.; Qiu, T.; Yan, W. Selective adsorption towards heavy metal ions on the green synthesized polythiophene/MnO_2 with a synergetic effect. *J. Cleaner Prod.* **2022**, *338*, 130536.

https://doi.org/10.1021/acsomega.4c03184
ACS Omega 2024, 9, 37012−37024

(33) Khalili, R.; Shabanpour, F.; Eisazadeh, H. Synthesis of polythiophene/Sb_2O_3 nanocomposite using sodium dodecylbenzenesulfonate for the removal of Pb (II). *Adv. Polym. Technol.* **2014**, *33* (2), 21389.
(34) Chen, J.; Zhu, J.; Wang, N.; Feng, J.; Yan, W. Hydrophilic polythiophene/SiO2 composite for adsorption engineering: Green synthesis in aqueous medium and its synergistic and specific adsorption for heavy metals from wastewater. *Chem. Eng. J.* **2019**, *360*, 1486−1497.
(35) Chetia, R.; Devi, S.; Bordoloi, S.; Pokhrel, B.; Shukla, N.; Gogoi, A.; Konwer, S. One-Step Synthesis of Polythiophene as a Potential Adsorbent for Removal of As (III) and As (V) from Aqueous Solution. *Water, Air, Soil Pollut.* **2023**, *234* (6), 369.
(36) Bora, C.; Pegu, R.; Saikia, B. J.; Dolui, S. K. Synthesis of polythiophene/graphene oxide composites by interfacial polymerization and evaluation of their electrical and electrochemical properties. *Polym. Int.* **2014**, *63* (12), 2061−2067.
(37) Ma, F.; Zhao, B.; Diao, J.; Jiang, Y.; Zhang, J. Mechanism of phosphate removal from aqueous solutions by biochar supported nanoscale zero-valent iron. *RSC Adv.* **2020**, *10* (64), 39217−39225.
(38) Wu, C.; Tu, J.; Liu, W.; Zhang, J.; Chu, S.; Lu, G.; Lin, Z.; Dang, Z. The double influence mechanism of pH on arsenic removal by nano zero valent iron: electrostatic interactions and the corrosion of Fe°. *Environ. Sci.: Nano* **2017**, *4* (7), 1544−1552.
(39) Shukla, S.; Jadaun, A.; Arora, V.; Sinha, R. K.; Biyani, N.; Jain, V. K. In vitro toxicity assessment of chitosan oligosaccharide coated iron oxide nanoparticles. *Toxicol. Rep.* **2015**, *2*, 27−39.
(40) Wang, Y.; Gai, L.; Ma, W.; Jiang, H.; Peng, X.; Zhao, L. Ultrasound-assisted catalytic degradation of methyl orange with Fe_3O_4/polyaniline in near neutral solution. *Ind. Eng. Chem. Res.* **2015**, *54* (8), 2279−2289.
(41) Singh, R.; Bajpai, A. K.; Shrivastava, A. K. CdSe nanorod-reinforced poly (thiophene) composites in designing energy storage devices: study of morphology and dielectric behavior. *Polym. Bull.* **2021**, *78*, 115−131.
(42) Amruth, K.; Abhirami, K. M.; Sankar, S.; Ramesan, M. T. Synthesis, characterization, dielectric properties and gas sensing application of polythiophene/chitosan nanocomposites. *Inorg. Chem. Commun.* **2022**, *136*, 109184.
(43) Liu, A.; Liu, J.; Pan, B.; Zhang, W. X. Formation of lepidocrocite (γ-FeOOH) from oxidation of nanoscale zero-valent iron (nZVI) in oxygenated water. *RSC Adv.* **2014**, *4* (101), 57377−57382.
(44) Panda, A. P.; Rout, P.; Kumar, S. A.; Jha, U.; Swain, S. K. Enhanced performance of a core−shell structured Fe(0)@Fe oxide and Mn(0)@Mn oxide (ZVIM) nanocomposite towards remediation of arsenic contaminated drinking water. *J. Mater. Chem. A* **2020**, *8* (8), 4318−4333.
(45) Kumar, A. S. K.; Jiang, S. J. Chitosan-functionalized graphene oxide: A novel adsorbent an efficient adsorption of arsenic from aqueous solution. *J. Environ. Chem. Eng.* **2016**, *4* (2), 1698−1713.
(46) Akoto, J. D.; Chai, F.; Repo, E.; Yang, Z.; Wang, D.; Zhao, F.; Liao, Q.; Chai, L. Polyethyleneimine stabilized nanoscale zero-valent iron-magnetite (Fe_3O_4@ nZVI-PEI) for the enhanced removal of arsenic from acidic aqueous solution: Performance and mechanisms. *J. Environ. Chem. Eng.* **2022**, *10* (6), 108589.
(47) Schmidt, M. W.; Baldridge, K. K.; Boatz, J. A.; Elbert, S. T.; Gordon, M. S.; Jensen, J. H.; Koseki, S.; Matsunaga, N.; Nguyen, K. A.; Su, S.; Windus, T. L. General atomic and molecular electronic structure system. *J. Comput. Chem.* **1993**, *14* (11), 1347−1363.
(48) Barca, G. M. J.; Bertoni, C.; Carrington, L.; Datta, D.; De Silva, N.; Deustua, J. E.; Fedorov, D. G.; Gour, J. R.; Gunina, A. O.; Guidez, E.; et al. Recent developments in the general atomic and molecular electronic structure system. *J. Chem. Phys.* **2020**, *152* (15), 154102−154125.

https://doi.org/10.1021/acsomega.4c03184
ACS Omega 2024, 9, 37012−37024